Z-scan and spatial self-phase modulation of a Gaussian beam in a thin nonlocal nonlinear media

Z-scan and spatial self-phase modulation of a Gaussian beam in a thin nonlocal nonlinear media

E V Garcia Ramirez[1], M L Arroyo Carrasco[1], M M Mendez Otero[1], E Reynoso Lara[2], S Chavez-Cerda[3] and M D Iturbe Castillo[3]

[1] Facultad de Ciencias Físico-Matemáticas, Benemérita Universidad Autónoma de Puebla, Avenida San Claudio y 18 Sur. Col San Manuel, CP 72570, Puebla, Puebla, Mexico
[2] Facultad de Ciencias de la Electrónica, Benemérita Universidad Autónoma de Puebla, Avenida San Claudio y 18 Sur. Col San Manuel, CP 72570, Puebla, Puebla, Mexico
[3] Instituto Nacional de Astrofísica, Óptica y Electrónica, Luis Enrique Erro # 1, CP 72840 Tonantzintla, Puebla, Mexico

E-mail: emma_vgr@yahoo.com.mx

Abstract

Considering that the nonlinear photoinduced phase shift to a Gaussian beam in a thin sample of nonlocal nonlinear media can be modeled as a Gaussian function to some real power the far-field can be calculated using the Fraunhofer integral. In this paper we calculate numerically this integral to obtain the on-axis intensity in a Z-scan experiment or the intensity pattern in a self-phase modulation experiment. Experimental results of samples under cw illumination are fitted using the model with a good correspondence between experimental and numerical results. The model presented is adequate to describe samples with any magnitude of the maximum nonlinear photoinduced phase shift of purely refractive local or nonlocal nonlinear thin media.

Keywords: nonlinear phase shift, nonlocal nonlinear media, Z-scan, self-phase modulation

1. Introduction

The Z-scan technique to evaluate the nonlinear refractive index of materials was proposed by Sheik-Bahae *et al* in 1989 [1]. Its popularity has increased since then due to its experimental simplicity and easy analysis of the results to give the sign and magnitude of the nonlinear index change. Originally the technique was proposed with a Gaussian beam and for on-axis intensity detection, for thin nonlinear samples and small photoinduced phase shifts ($< \pi$) [2]. Later, thick samples were considered in the technique [3], and off-axis or eclipsed detection was proposed in order to increase the sensitivity [4, 5]. Different incident beam shapes have also been considered like top-hat [6], non-Gaussian [7], circularly symmetric [8] and arbitrary beams [9]. With the development of light sources with femtosecond pulse duration the scope of the Z-scan technique was increased to use white-light continuum for characterization of degenerate nonlinear absorption and refraction [10], for the

simultaneous measurement of self-phase modulation and two-photon absorption with shaped femtosecond laser pulses [11], and for the investigation of the temporal duration of the third-order nonlinear refraction induced by a given laser pulse [12].

The Z-scan technique can be considered as an extension of the extracavity thermal lens technique of Hu and Whinnery [13], a technique used to evaluate low absorptivity in liquids [14, 15]. A theoretical model of the laser-induced thermal lens taking into account the aberrant nature of the lens was presented in [16]. In [17] the refractive shape of the thermal lens was approximated with a parabola and was compared with the aberrant model and experimental results. The most complete model to study the effect of an aberrant thermal lens was presented in [18], where the exact diffraction integral is calculated: however, an approximation was made in the temperature field.

The Z-scan technique from the theoretical point of view, in order to calculate the on-axis intensity at far-field, has been treated with the Gaussian beam decomposition (GD)

method [2, 19], the Huygens–Fresnel principle [20], the diffraction theory [21] and other methods. Recently, it was demonstrated that the GD approach can be used to describe samples with large nonlinear phase shifts ($>\pi$) [22]. The main result obtained with this theory, for small nonlinear phase shifts, was an analytical formula for the on-axis normalized transmittance T of the form

$$T = 1 + \frac{4\Delta\Phi_0 x}{(x^2+1)(x^2+9)} \quad (1)$$

where $x = z/z_0$, $z_0 = \pi w_0^2/\lambda$, w_0 is the waist of the incident Gaussian beam of wavelength λ and $\Delta\Phi_0$ is the nonlinear phase shift at the waist. The curve described by equation (1) has a peak–valley transmittance difference given by $\Delta T_{p-v} = 0.406|\Delta\Phi_0|$ and a peak–valley separation of $\Delta z_{p-v} = 1.72z_0$. However, different expressions have been proposed in order to describe the results obtained for materials with a nonlocal response. For example, in [23], for a model based on a thermal medium a $\Delta T_{p-v} = 2|\Delta\Phi_0|$ and $\Delta z_{p-v} = 2z_0$ were calculated.

Recently, a general Z-scan theory based on the solution of the paraxial wave equation and the Huygens–Fresnel principle was presented [24]. It was demonstrated that equation (1) is valid for $|\Delta\Phi_0| < 0.2\pi$ rad and they made a comparison between different models, concluding that models that do not apply the parabolic approximation give correct results. However, the results obtained in that paper are valid only in the case of materials with a local response.

In this work we demonstrate numerically that the relations obtained with the GD model are valid only when the response of the material is local. When the nonlocality of the nonlinear material response is taken into account then different dependences need to be considered without regarding the magnitude of the on-axis nonlinear phase shift. Our results are based on the recently published model where a simple expression was given to consider the nonlocality in spatial self-phase modulation experiments [25]. Our main idea is to consider that the spatial extension of the photoinduced nonlinear phase shift can be wider or narrower than the incident intensity beam. This idea had been used in order to obtain a good correspondence between experimental and theoretical results in spatial self-phase modulation experiments in materials as liquid crystals [26] and dyed solutions [27]. We show how the changes of ΔT_{p-v} and Δz_{p-v} are functions of both the nonlocality of the material and the magnitude of $\Delta\Phi_0$.

In section 2 we present our theoretical model where a dependence on z is included in the on-axis nonlinear phase shift in order to describe Z-scan results with the same model. Analyses for small and large phase shifts are presented in the following sections. Experimental results for different materials under cw illumination are adjusted using the proposed model. Finally the conclusions are given.

2. Theoretical model

We consider a Gaussian beam of waist w_0 and wavelength λ, propagating in the z direction. This beam has a Rayleigh range

z_0 given by $z_0 = \pi w_0^2/\lambda$, and the following field amplitude:

$$E(r, z) = A_0 \frac{w_0}{w(z)} \exp\left[-\frac{r^2}{w(z)^2}\right] \exp\left[-ikz - ik\frac{r^2}{2R(z)} + i\varepsilon(z)\right] \quad (2)$$

where

$$w(z) = w_0[1 + (z/z_0)^2]^{1/2} \quad (3)$$

$$R(z) = z[1 + (z_0/z)^2] \quad (4)$$

$$\varepsilon(z) = \tan^{-1}(z/z_0) \quad (5)$$

where A_0 is a constant, $k = 2\pi/\lambda$, $w(z)$ and $R(z)$ are the beam width and wavefront radius of curvature, respectively, and $\epsilon(z)$ is the Gouy phase retardation relative to a plane wave.

At some distance z, from the waist, the beam illuminates an optical nonlinear sample of width d. The sample is going to be considered as thin ($d \ll z_0$) and that presents a refractive index dependent on the incident intensity. It is well accepted that when a Gaussian beam illuminates such a sample then the output field can be expressed by [28]

$$E_{\text{out}} = E(r, z) \exp(-i\Delta\phi(r)) \quad (6)$$

where we are considering for simplicity that the sample does not have absorption. E is the field amplitude of the Gaussian beam at the entrance of the sample, r the radial coordinate and $\Delta\phi(r)$ the nonlinear phase change. In order to obtain this approximation it is necessary to consider that the incident beam amplitude does not change inside the media. This can be demonstrated considering the nonlinear Schrödinger equation where the transversal Laplacian can be ignored. For example, for a Gaussian beam, if a 5% change in the beam radius is allowed that means that the approximation is valid for a width smaller than $z_0/3$. We propose that this nonlinear phase change can be approximated as

$$\Delta\phi(r) \approx \Delta\phi_0(z, m) \exp(-mr^2/w(z)^2) \quad (7)$$

where

$$\Delta\phi_0(z, m) = \frac{\Delta\Phi_0}{(1 + (z/z_0)^2)^{m/2}} \quad (8)$$

where $\Delta\Phi_0$ is the maximum on-axis photoinduced phase shift in the beam after the nonlinear medium located at $z = 0$ and m can be any real positive number. An analogous approach has been used by other groups in order to explain their experimental results: a corresponding value of $m = 3.7$ was used in [26] and m values around 1 were used in [27]. As discussed in [25], only for $m = 2$ the nonlinear phase change follows the intensity distribution and then the response of the material is considered as local, values of m different from two will be considered as nonlocal. This dependence for the nonlinear phase shift, for $m = 2$, has also been considered in [20]. It is important to note that, without the dependence on z in the nonlinear phase change (8), it is impossible to describe the on-axis intensity in the Z-scan technique.

Both the Z-scan technique and spatial self-phase modulation experiments require detection at far-field. Then in our case, the field distribution at that plane can be calculated from the Fraunhofer integral using equation (6) as the input
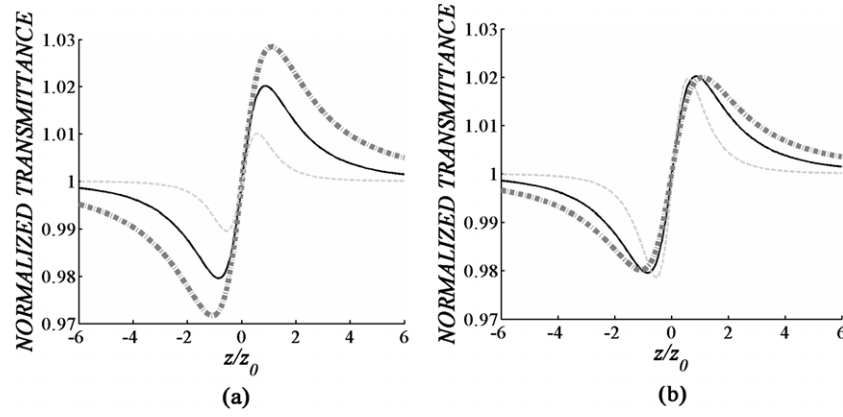
Figure 1. *Z*-scan curves obtained for: (a) the same on-axis nonlinear phase shift of 0.1 rad and different values of the parameter *m*: 1 (square line), 2 (solid line) and 4 (dotted line), and (b) different values of $\Delta\Phi_0 = 0.07$ rad ($m = 1$, square line), 0.10 rad ($m = 2$, solid line) and 0.2 rad ($m = 4$, dotted line).
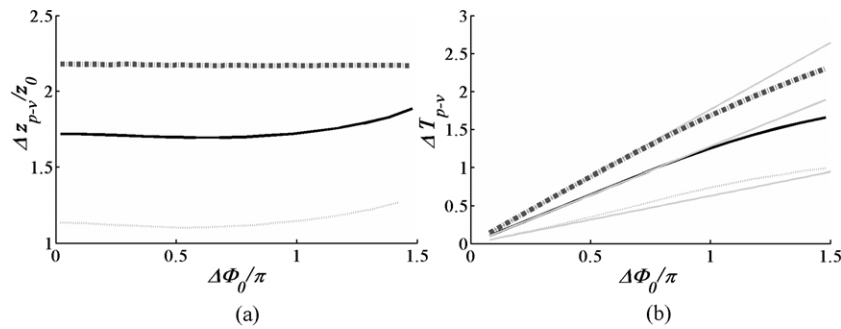

Figure 2. Numerical results for: (a) $\Delta z_{p-v}/z_0$ and (b) ΔT_{p-v} as functions of $\Delta\Phi_0$, for *m* equal to: 1 (square line), 2 (solid line) and 4 (dotted line). Gray solid lines represent a linear behavior for small $\Delta\Phi_0$.

field. This integral is obtained numerically in this paper to calculate the on-axis intensity or the cross section.

In section 3 we present numerical results for the Fourier transform of the field given by equation (6), considering equation (8), for nonlinear phase shifts smaller than π and different values of *m* in the *Z*-scan technique. Next, *Z*-scan results are presented for large values of the nonlinear phase shift and in some positions the intensity pattern is shown.

3. Numerical results

3.1. Nonlinear phase shifts smaller than π

When $\Delta\Phi_0 < \pi$ rad, very few rings appear at far-field; then it is more usual to represent the nonlinear behavior of any sample using the *Z*-scan technique. In figure 1(a) the *Z*-scan curves obtained for a sample with $\Delta\Phi_0 = 0.1$ rad are plotted for different values of the parameter *m*. For $m = 2$, the obtained curve is very similar to that given by equation (1). However, when $m < 2$ the amplitude of the curve is larger than that obtained for the local case and for $m > 2$ the amplitude of the curve is smaller than that for the local case. At first sight it seems that no large differences appear in the *Z*-scan curves. However, in order to see clearly the main differences between the curves, in figure 1(b) are shown the *Z*-scan curves for *m* values of: 1, 2 and 4, but values of $\Delta\Phi_0$ were adjusted to give

almost the same peak–valley transmittance difference. In this figure we can observe that the curves differ in the peak–valley position and in the form of how the transmittance behaves far from $z = 0$. Then different values of the parameter *m* give *Z*-scan curves with particular characteristics.

In particular when $m = 2$, local case (solid lines), the peak–valley separation distance as a function of $\Delta\Phi_0$ follows a behavior as that shown in figure 2(a) (solid line). This behavior is very similar to that reported when an analytical expression is obtained for the on-axis normalized transmittance in a *Z*-scan experiment [29]. For small nonlinear phase shifts the separation takes the value obtained by Sheik-Bahae of $1.72z_0$: however, the separation rapidly reached a minimum value of $1.69z_0$ at $\Delta\Phi_0 = 0.6\pi$ rad and for values of $\Delta\Phi_0 > \pi$ rad the separation increased monotonically. The peak–valley transmittance difference ΔT_{p-v} followed the behavior shown in figure 2(b) (solid line), where the gray solid line represents the results obtained from the GD method. One more time, our results are very similar to those obtained with the analytical formula presented in [20]. As we can observe the results from the GD method are valid for $\Delta\Phi_0 < \pi$ rad.

For $m = 1$, this means a medium where the locality of the nonlinearity extends beyond the illuminated region. The characteristics of the *Z*-scan curve for $\Delta\Phi_0 < \pi$ rad are the following: the Δz_{p-v} is $2.2z_0$ for very small phases and it remains practically constant for $\Delta\Phi_0 < 1.5\pi$ rad, square line
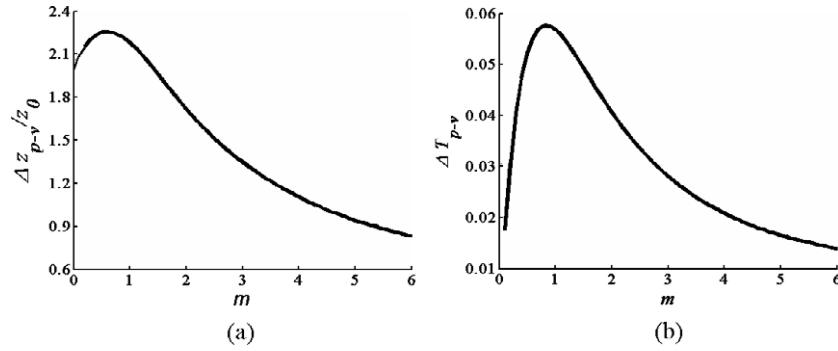
Figure 3. Numerical results for: (a) $\Delta z_{\mathrm{p-v}}/z_0$ and (b) $\Delta T_{\mathrm{p-v}}$ as functions of the parameter m for $\Delta \Phi_0 = 0.1$ rad.

in figure 2(a). Note that this peak–valley separation distance is very similar to that obtained in Z-scan experiments with cw excitation of dyed solutions [29] and theoretical Z-scan curves with a dependence in the photoinduced focal length to the square of the beam radius [30]. The peak–valley transmittance difference is plotted as the square line in figure 2(b), where we can observe that a linear behavior is obtained for $\Delta \Phi_0 < \pi/2$ rad, with a dependence given by $\Delta T_{\mathrm{p-v}} = 0.56|\Delta \Phi_0|$; this means that for this nonlocality the amplitude of the curve is larger than that for a local media, for the same $\Delta \Phi_0$. For $\Delta \Phi_0 > \pi/2$ rad, the peak–valley difference is smaller than the linear prediction.

For $m = 4$, this means a material where the nonlinear phase shifts take up an area smaller than the incident beam; the results obtained for the peak–valley separation and transmittance difference are shown as dashed lines in figure 2. For small nonlinear phase shifts the separation takes the value of $1.13z_0$, reached a minimum of $1.10z_0$ at $\Delta \Phi_0 = 0.6\pi$ rad and after that the separation increases monotonically. Note that this difference is almost $1/2$ of that obtained with $m = 1$ and $1/3$ smaller than that obtained with $m = 2$. The peak–valley transmittance difference followed a behavior as that shown in figure 2(b) (dashed line). We can observe a linear behavior for nonlinear phases smaller than 0.3π rad, with a dependence of the form $\Delta T_{\mathrm{p-v}} = 0.2|\Delta \Phi_0|$. For higher values than 0.3π rad of the nonlinear phase the difference is larger than that predicted by the linear behavior.

From the values used as an example to see the influence of m in the Z-scan curve it seems that $m < 2$ produces Z-scan curves with a peak–valley separation larger than that obtained with $m = 2$ and the opposite for $m > 2$. However, this is not the case: the peak–valley separation distance does not increase to infinity as m decreases, it reaches a maximum value for $m = 0.6$, see figure 3(a), and tends to zero as m increases in a very slow way. Similar behavior is obtained for the peak–valley transmittance difference: a maximum is obtained for $m = 0.8$ and tends to zero as m increases in a very slow way, see figure 3(b).

From the previous analysis, we can say that it is not enough to have, from a Z-scan curve, the peak–valley separation distance and the peak–valley transmittance difference because more than one m value gives such characteristics. It is important to also reproduce the behavior of the transmittance far from $z = 0$. For example, if a separation
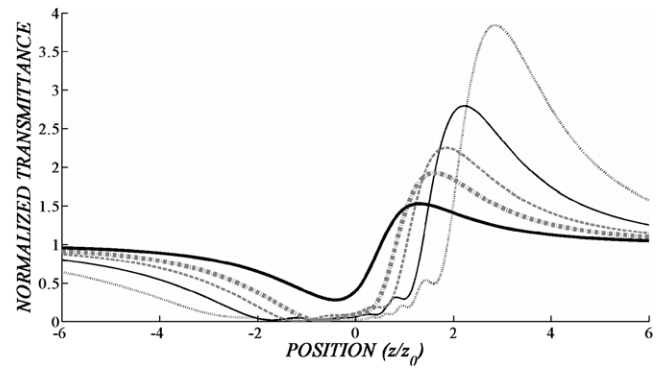

Figure 4. Z-scan curves for the local case ($m = 2$) and $\Delta \Phi_0$ of: π (thick black line), 2π (square line), 3π (dashed line), 5π (thin black line) and 10π (dotted line) rad.

of $2.1z_0$ is obtained for a sample in some Z-scan experiment, then two values of m reproduce such a separation. To decide which value is adequate it is important to know all the behavior in z of the normalized transmittance.

In order to calculate the normalized transmittance in our model when $\Delta \Phi_0 < \pi/2$ rad, the following empirical formula can be used:

$$T(z) = 1 + \frac{2m\Delta \Phi_0 x}{(x^2 + (m+1)^2)(x^2 + 1)^{m/2}} + \frac{m^2(3x^2 - (2m+1))\Delta \Phi_0^2}{(x^2 + 1)^m (x^2 + (m+1)^2)(x^2 + (2m+1)^2)} \quad (9)$$

where $x = z/z_0$. When $m = 2$ this formula reproduces the expression obtained under a second-order approximation for pure third-order nonlinear refraction, using the Gaussian decomposition method [31].

3.2. Nonlinear phase shifts larger than π

When the nonlinear phase shift is larger than π, the Z-scan curves begin to be asymmetric and the peak–valley separation increases. In figure 4 we plot the normalized transmittance for different $\Delta \Phi_0$ for the local case ($m = 2$). In this case the peak moved to positive values in a faster way than the valley moved to negative values. The point of transmittance equal to one moved to positive values. The valley was broadening as the phase shift increased. Note that the curves for π, 2π
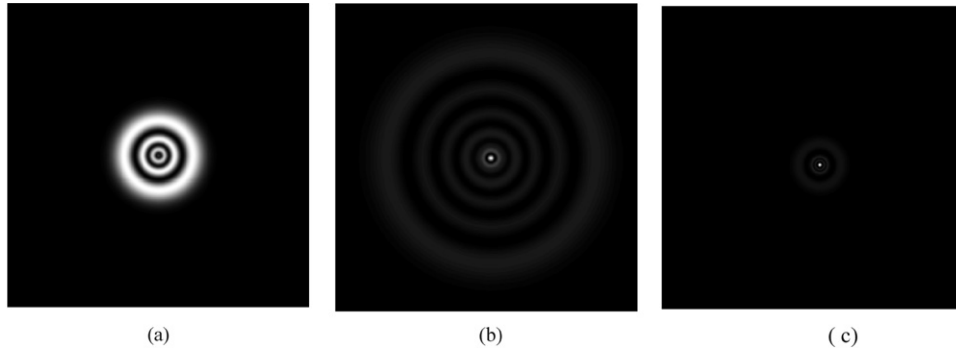
Figure 5. Cross sections of the far-field patterns versus angular position (ρ mm^{-1}) for the local case ($m = 2$) and $\Delta\Phi_0 = 10\pi$ rad at positions z: (a) $-z_0$, (b) 0 and (c) z_0.
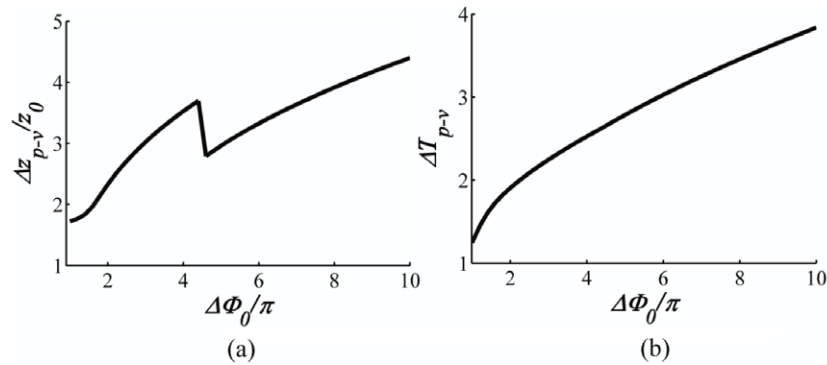

Figure 6. Numerically calculated (a) $\Delta z_{p-v}/z_0$ and (b) ΔT_{p-v} as functions of $\Delta\Phi_0$ for $m = 2$.

and 3π rad coincide with those presented in [20], where an analytical formula was used to calculate the on-axis normalized transmittance and are very similar to those presented in [21], where a diffraction model was used, and those in [22], where the Gaussian decomposition method was used. When $\Delta\Phi_0 > 2\pi$ rad some oscillation can be observed in the valley. This effect is due to the fact that the far-field intensity distribution consists of many rings and the center of the pattern is not completely dark for positions close to $z = 0$. Cross sections of the far-field patterns obtained for $\Delta\Phi_0 = 10\pi$ rad at positions $z = -z_0$, 0 and z_0 are plotted in figure 5, where the shown area is of 30×30 ρ^2 mm^{-2}. Note that very different intensity cross sections are obtained though a very similar normalized transmittance was obtained in the Z-scan curve for these points.

The behavior of the peak–valley separation distance and peak–valley transmittance difference as functions of $\Delta\Phi_0$ are shown in figure 6. In the first case we can observe that the separation increases as the nonlinear phase shift does. However, around $\Delta\Phi_0 = 4\pi$ rad there is a jump that is due to the oscillations of the intensity in the valley for large phase shifts. The peak–valley transmittance difference grows as the nonlinear phase shift does but with a tendency to saturation.

As an example of the nonlocal case with phase shifts larger than π and that extend beyond the incident intensity figure 7 shows the case $m = 1$. We present the results obtained for the normalized transmittance in a Z-scan experiment for different $\Delta\Phi_0$. Once again we can observe the asymmetry in the curve
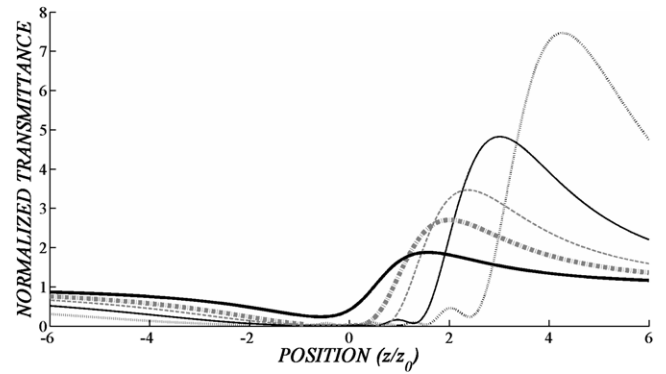

Figure 7. Z-scan curves for the nonlocal case ($m = 1$) and $\Delta\Phi_0$ of: π (thick black line), 2π (square line), 3π (dashed line), 5π (thin black line) and 10π (dotted line) rad.

for large phase shifts. The peak and valley in this case are much wider and the amplitude of the peak is larger than in the local one. Cross sections of the far-field patterns for the case of $\Delta\Phi_0 = 10\pi$ rad are presented in figure 8, where we can observe that, although the pattern at $z = -z_0$ is very similar to that obtained for the local case, the patterns in the other positions remarkably differ. The area of these sections is 30×30 ρ^2 mm^{-2} as for the case $m = 2$. The peak–valley separation distance and normalized transmittance as functions of $\Delta\Phi_0$ are plotted in figure 9, in the first case the separation presents sudden jumps due to the intensity oscillations that
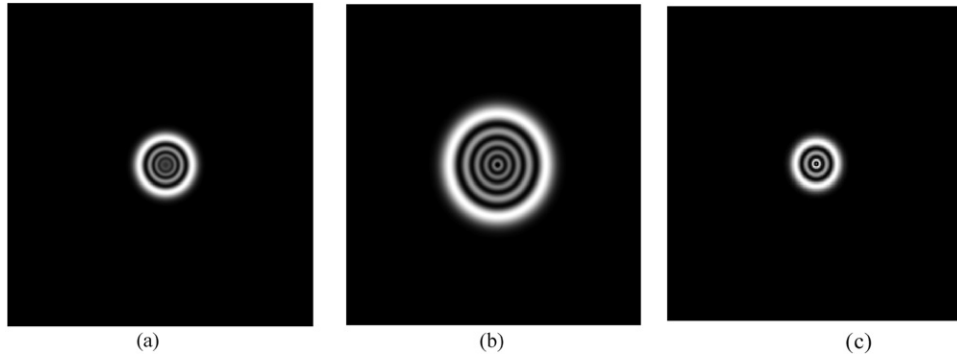
Figure 8. Cross sections of the far-field patterns versus angular position (ρ mm^{-1}) for a nonlocal sample ($m = 1$) and $\Delta\Phi_0 = 10\pi$ rad at positions: (a) $-z_0$, (b) 0 and (c) z_0.
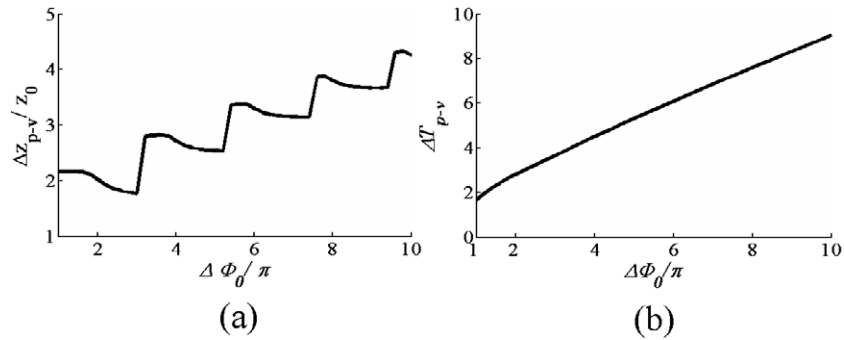

Figure 9. Numerically calculated (a) $\Delta z_{\mathrm{p-v}}/z_0$ and (b) $\Delta T_{\mathrm{p-v}}$ as functions of $\Delta\Phi_0$ for $m = 1$.

appear in the valley as the phase shift increases. The peak–valley normalized transmittance increases in a linear way, with a slope of 0.8, as the nonlinear phase shift grows.

As an example of the nonlocal case with a spatial extension smaller than the incident intensity we present in figure 10 the case $m = 4$, for phase shifts larger than π. The Z-scan curves are asymmetric as for the other m values. All the variations in the normalized transmittance are contained in the interval $-6z_0$ to $6z_0$. The valley is broader than the peak and the minimum intensity in the valley never reaches the zero value for larger phase shifts. The amplitude of the curve is smaller than that obtained for the local case. The cross sections of the far-field patterns obtained for positions $z = -z_0$, 0 and z_0 do not differ much, see figure 11.

The peak–valley separation distance and the normalized transmittance as functions of the nonlinear phase shifts are plotted in figure 12. In this case the peak–valley separation distance increases smoothly. Almost the same behavior is obtained for the peak–valley normalized transmittance difference. Both curves tend to saturation in a faster way than for the previous m values analyzed. For large phase shifts the Z-scan curves and the cross sections of the far-field patterns present very different features, depending on the m value.

Both peak–valley separation distance and peak–valley transmittance difference are plotted as functions of the parameter m for $\Delta\Phi_0$ of π and 5π rad in figure 13. We can observe that, for $\Delta\Phi_0 = \pi$ rad, the peak–valley separation distance follows the behavior obtained for small on-axis nonlinear phase shifts. However, for $\Delta\Phi_0 = 5\pi$ rad the curve
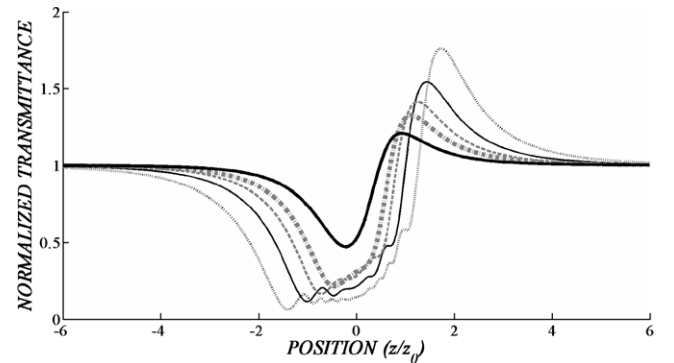

Figure 10. Z-scan curves for the nonlocal case ($m = 4$) and $\Delta\Phi_0$ of: π (thick black line), 2π (square line), 3π (dashed line), 5π (thin black line) and 10π (dotted line) rad.

presents sudden changes for values of $m < 2.2$. For values of $m > 2.2$ the separation decreases smoothly.

The peak–valley transmittance difference curves follow a similar behavior to that obtained for a small phase shift. For $\Delta\Phi_0 = 5\pi$ rad there is a maximum of 7.39 at $m = 0.5$ and the transmittance difference decays in an exponential way for larger values of m.

4. Experimental results fitting

In this section we present the fittings that can be obtained with the model presented for similar experimental conditions
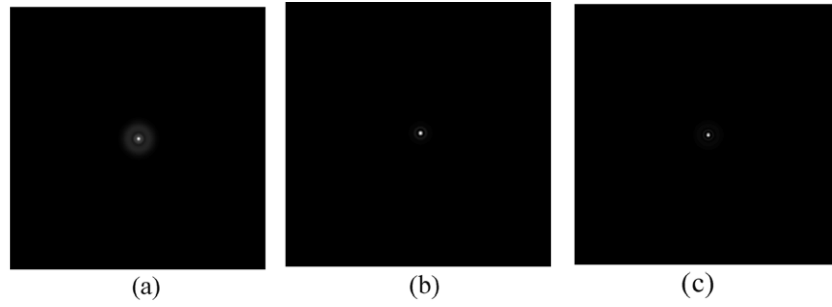
Figure 11. Cross sections of the far-field patterns versus angular position (ρ mm^{-1}) for a nonlocal sample ($m = 4$) and $\Delta\Phi_0 = 10\pi$ rad at positions: (a) $-z_0$, (b) 0 and (c) z_0.
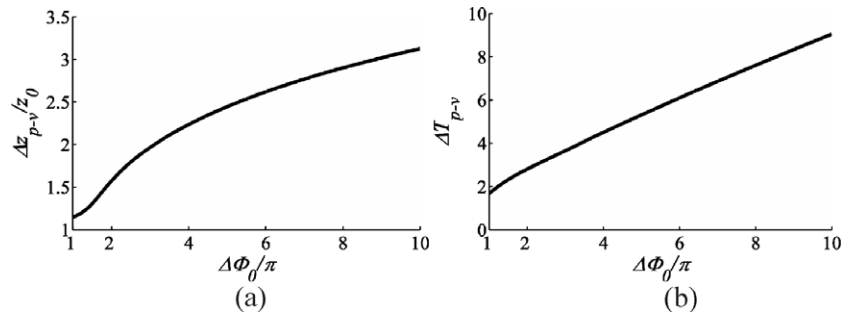

Figure 12. Numerically calculated (a) $\Delta z_{\mathrm{p-v}}/z_0$ and (b) $\Delta T_{\mathrm{p-v}}$ as functions of $\Delta\Phi_0$ for $m = 4$.

Figure 13. (a) $\Delta z_{\mathrm{p-v}}/z_0$ and (b) $\Delta T_{\mathrm{p-v}}$ as functions of m for $\Delta\Phi_0$ of: π (solid line) and 5π (square line) rad.

but different kinds of nonlinear media. In order to apply the model to the experiments we assume a thin sample and use the on-axis and far-field detection approximations. In the first case we present the experimental results reported in [29] for a dyed solution using a cw illumination from an He–Ne laser at 633 nm with a beam waist of $w_0 = 53$ μm. The behavior of the Z-scan curves for different incident powers (figure 6 [29]) of 6.6, 4.5, 2.8, 2.1 and 1.5 mW are shown in figure 14. Using our model with $m = 0.6$ and a beam waist of $w_0 = 67$ μm a good correspondence was obtained. The respective phase changes for the simulations were the following $\Delta\Phi_0$: -7.2, -3.5, -2.8, -1.9 and -1.4 rad. Due to the experimental conditions it is well accepted that for this material the exhibited nonlinearity must be thermal [29].

The value of the parameter m used for fitting the experimental results predicts a $\Delta z_{\mathrm{p-v}}/z_0$ of 2.2 for small $\Delta\Phi_0$,

which is larger than that assumed in [29]. However, the model presented here produces a better fit with the experimental results for the different incident powers. Note that the value used for $\Delta\Phi_0$ in rad is very close to the value of the incident intensity, demonstrating that they are directly related. In order to exhibit the agreement of the empirical formula (9), for small values of $\Delta\Phi_0$, in figure 15 we show the same experimental results, of figure 14, fitted with equation (9), for $m = 0.6$ and $\Delta\Phi_0$: -2.8 (gray dashed line), -1.9 (thin black line) and -1.4 (dotted line) rad. We can observe that for $\Delta\Phi_0$: -1.9 and -1.4 rad the fitted curves adjust very well with the experimental results. For $\Delta\Phi_0 = -2.8$ rad there is not a good correspondence with the experimental results, due to the formula (9) not being adequate for large phase shifts.

As a second set of experimental results to be adjusted with the model, we present that reported in [32], where
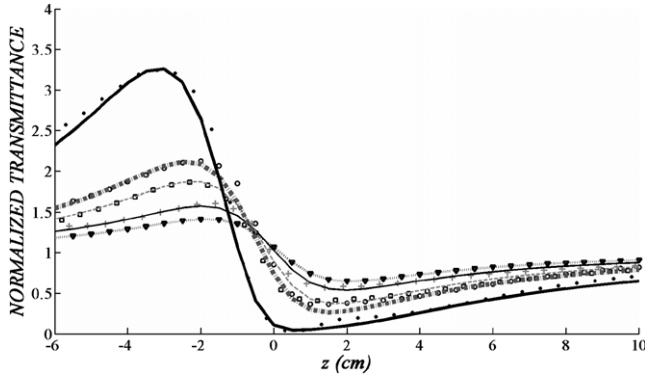
Figure 14. Experimental results reported in [29] figure 6, for a dyed solution illuminated with an He–Ne laser beam at 633 nm and the following incident powers: 6.6 (dot), 4.5 (circle), 2.8 (square), 2.1 (+) and 1.5 (triangle) mW. Lines are the best fitting obtained with $m = 0.6$ and $\Delta\Phi_0$: -7.2 (black), -3.5 (square line), -2.8 (gray dashed line), -1.9 (thin black line) and -1.4 (dotted line) rad.

Figure 16. Z-scan curves for a planar cell of dye doped 5CB liquid crystal (figure 1, [32]) as a function of the incident polarization: $0°$ (dot), $30°$ (circle), $60°$ (square) and $90°$ (+), with respect to the director vector. Continuous lines are fittings obtained for $m = 1$ and polarizations of: $0°$ (thick black line), $30°$ (dashed line), $60°$ (dotted line) and $90°$ (thin black line).
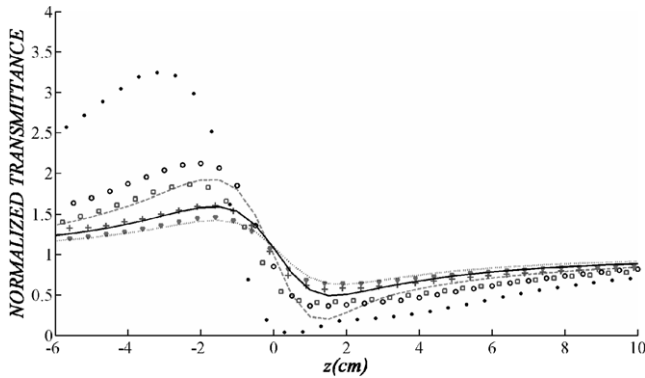

Figure 15. Experimental results reported in [29] figure 6, for a dyed solution illuminated with an He–Ne laser beam at 633 nm and the following incident powers: 6.6 (dot), 4.5 (circle), 2.8 (square), 2.1 (+) and 1.5 (triangle) mW. Lines are the fitting curves obtained with empirical equation (9) for $m = 0.6$ and $\Delta\Phi_0$: -2.8 (gray dashed line), -1.9 (thin black line) and -1.4 (dotted line) rad.

Figure 17. Z-scan curves obtained with $m = 2$ (thick line) and $m = 1$ (thin line). Black dots are experimental results for a polarization of $0°$ (figure 1, [32]).

a sample of 5CB liquid crystal with methyl red dye in a planar configuration is characterized using a cw He–Ne laser beam at 633 nm with a beam waist of $w_0 = 20$ μm. This sample presented Z-scan curves that depend on the incident polarization: parallel to the director vector, the sample exhibits a negative nonlinear behavior and, with orthogonal polarization, the sample exhibits a positive one. The experimental results for different incident polarizations ([32], figure 1) are shown in figure 16 for an incident power of 4 mW. In this case the experimental results can be fitted using a parameter value of $m = 1$ and two different values of the maximum photoinduced phase shift in the sample, one for the negative response of $\Delta\Phi_{0-} = -6.6$ rad and $\Delta\Phi_{0+} = 0.3$ rad for the positive case. The beam waist was assumed to be of 16 μm. Note that the fitting for the curve at zero degrees reproduces very well the experimental points for values of $z < 0.3$ cm. However, some discrepancies appear for values of $z > 0.3$ cm. In this case we think that more than one
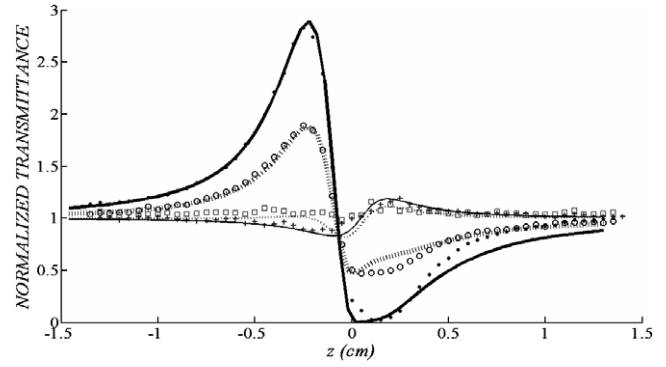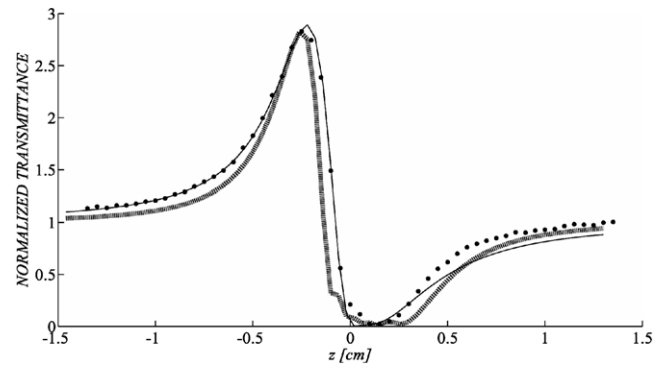
nonlinear response is exhibited by the sample and a more elaborated model must be proposed in order to obtain a better correspondence with the experiment. As a comparison with the fitting, considering that the response of the material is local, we present the best fitting for $m = 2$ and that obtained with $m = 1$, see figure 17. We notice that our model has an overall better fitting compared to that corresponding to the local case of $m = 2$.

Finally, with the model it is also possible to describe qualitatively experimental results reported for gold nanoparticles in cyclohexanone, under cw radiation at 532 nm [33]. The ringed far-field patterns and Z-scan curve with large amplitude were obtained. The corresponding numerical results are shown in figures 18 and 19 for values of $m = 0.4$ and $\Delta\Phi_0 = -9.5\pi$ rad. In [33] the author mentions that they tried to model their experimental results using the aberrant thermal lens model. However, the simulations differ from the experimental results. With our model the correspondence between the Z-scan curve and the experimental results, reported in [33] figure 9, is very good along the amplitude of the curve and the position of the maxima and minima. Note that the cross section
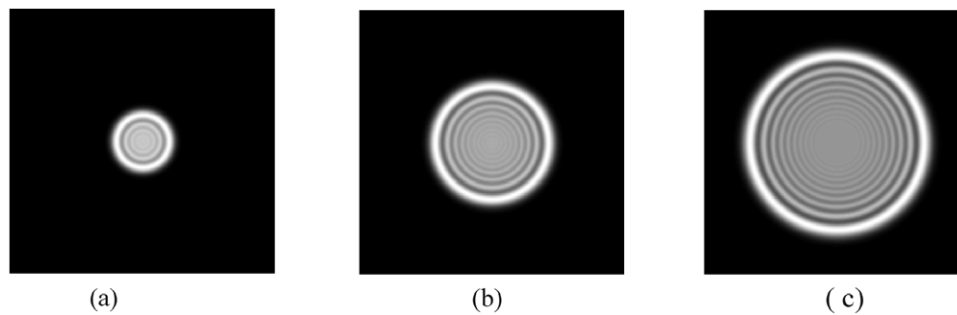
Figure 18. Numerical cross sections of the far-field patterns versus angular position (ρ mm^{-1}) for a sample located at the waist of a Gaussian beam with $\Delta\Phi_0$ of: (a) -10π, (b) -20π and (c) -30π rad for $m = 0.4$.
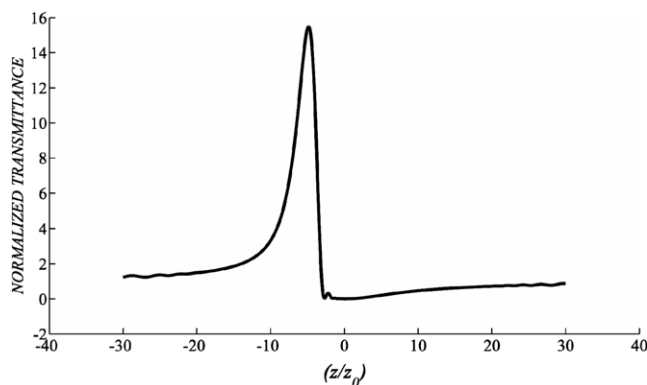

Figure 19. Numerical Z-scan curve obtained for a sample with $\Delta\Phi_0 = -9.5\pi$ rad and $m = 0.4$.

obtained numerically and the experimental results are in good correspondence considering that the phase and the power are directly related ([24], figure 10).

5. Conclusions

In this paper we have presented a simple model to calculate, in a numerical way, the on-axis far-field intensity in a Z-scan experiment or the far-field pattern in a spatial self-phase modulation experiment, where a Gaussian beam was used and a thin nonlocal nonlinear medium with a refractive nonlinearity was analyzed. We demonstrate that the peak–valley separation distance and the transmittance difference in a Z-scan experiment depended on the locality in the nonlinear response of the sample. The formulae obtained in the literature with different approaches for the normalized transmittance are valid only for the local case. When the material presents a nonlocal response, then different dependences for $\Delta z_{\mathrm{p-v}}$ and $\Delta T_{\mathrm{p-v}}$ as functions of $\Delta\Phi_0$ are obtained, according to our model. With this model it was possible to adjust numerically, with a good correspondence, experimental results for large phase shifts and a large nonlocal nonlinear response for different kinds of materials. The model can be used to calculate off-axis or eclipsing Z-scans. Materials with more than one nonlocal process can also be considered. The model presented here can be extended in order to consider nonlinear

absorption and the influence of more than one effect in the nonlinear response of the material.

References

[1] Sheik-Bahae M, Said A A and Van Stryland E W 1989 High-sensitivity, single-beam n_2 measurements *Opt. Lett.* **14** 955–7

[2] Sheik-Bahae M, Said A A, Wei T H, Hagan D J and Van Stryland E W 1990 Sensitive measurement of optical nonlinearities using a single beam *IEEE J. Quantum Electron* **26** 760–9

[3] Sheik-Bahae M, Said A A, Hagan D J, Soileau M J and Van Stryland E W 1991 Nonlinear refraction and optical limiting in thick media *Opt. Eng.* **30** 1228–35

[4] Xia T, Hagan D J, Sheik-Bahae M and Van Stryland E W 1994 Eclipsing Z-scan measurement of $\lambda/104$ wavefront distortion *Opt. Lett.* **19** 317–19

[5] Tian J G, Zang W P and Zhang G 1994 Two modified Z-scan methods for determination of nonlinear-optical index with enhanced sensitivity *Opt. Commun.* **107** 415–9

[6] Zhao W and Palffy-Muhoray P 1993 Z-scan technique using top-hat beams *Appl. Phys. Lett.* **63** 1613–5

[7] Bridges R E, Fisher G I and Boyd R W 1995 Z-scan measurement technique for non-Gaussian beams and arbitrary sample thicknesses *Opt. Lett.* **20** 1821–3

[8] Rhee B K, Byun J S and Van Stryland E W 1995 Z-scan measurement technique for non-Gaussian beams and arbitrary sample thicknesses *Opt. Lett.* **20** 1821–3

[9] Zang W P, Tian J G, Lui Z B, Zhou W Y, Song F and Zhang C P 2004 Local one-dimensional approximation for fast simulation of Z-scan measurements with an arbitrary beam *Appl. Opt.* **43** 4408–14

[10] Balu M, Hales J, Hagan D J and Van Strayland E W 2004 White-light continuum Z-scan technique for nonlinear materials characterization *Opt. Express* **12** 3820–6

[11] Fisher M C, Liu H C, Piletic I R and Warren W S 2008 Simultaneous self-phase modulation and two-photon absorption measurement by a spectral homodyne Z-scan method *Opt. Express* **16** 4192–05

[12] Gu B, Wang H T and Ji W 2009 Z-scan technique for investigation of the noninstantaneous optical Kerr nonlinearity *Opt. Lett.* **34** 2769–71

[13] Hu C and Whinnery J R 1973 New thermooptical measurements method and a comparison with other methods *Appl. Opt.* **12** 72–9

[14] Leite R C C, Moore R S and Whinnery J R 1964 Low absorption measurements by means of the thermal lens effect using an He–Ne laser *Appl. Phys. Lett.* **5** 141–3

[15] Gordon J P, Leite R C C, Moore R S, Porto S P S and Whinnery J R 1965 Long-transient effects in lasers with inserted liquid samples *J. Appl. Phys.* **36** 3–8

[16] Sheldon S J, Knight L V and Thome J M 1982 Laser-induced thermal lens effect: a new theoretical model *Appl. Opt.* **21** 1663–9

[17] Carter C A and Harris J M 1984 Comparison of models describing the thermal lens effect *Appl. Opt.* **23** 476–81

[18] Jürgensen F and Schröer W 1995 Studies on the diffraction image of a thermal lens *Appl. Opt.* **34** 41–50

[19] Weaire D, Wherrett B S, Miller D A B and Smith S D 1979 Effect of low-power nonlinear refraction on laser-beam propagation in InSb *Opt. Lett.* **4** 331–3

[20] Samad R E and Vieira N D Jr 1998 Analytical description of Z-scan on-axis intensity based on the Huygens–Fresnel principle *J. Opt. Soc. Am.* B **15** 2742–7

[21] Yao B, Ren L and Hou X 2003 Z-scan theory based on a diffraction model *J. Opt. Soc. Am.* B **20** 1290–4

[22] Chen S Q, Liu Z B, Zang W P, Tian J G, Zhou W Y, Song F and Zhang C P 2005 Study on Z-scan characteristics for a large nonlinear phase shift *J. Opt. Soc. Am.* B **22** 1911–6

[23] Cuppo F L S, Figueiredo Neto A M, Gomez S L and Palffy-Muhoray P 2002 Thermal-lens model compared with the Sheik-Bahae formalism in interpreting Z-scan experiments on lyotropic liquid crystals *J. Opt. Soc. Am.* B **19** 1342–8

[24] Pálfalvi L, Tóth B C, Almási G, Fülöp J A and Hebling J 2009 A general Z-scan theory *Appl. Phys.* B **97** 679–85

[25] Garcia Ramirez E V, Arroyo Carrasco M L, Mendez Otero M M, Chavez Cerda S and Iturbe Castillo M D 2010 Far field intensity distributions due to spatial self phase modulation of a Gaussian beam by a thin nonlocal nonlinear media *Opt. Express* **18** 22067–79

[26] Durbin S D, Arakelian S M and Shen Y R 1981 Laser induced diffraction rings from a nematic liquid crystal film *Opt. Lett.* **6** 411–3

[27] Yokota Y, Ogusu K and Tanaka Y 1998 Focused-beam-induced diffraction rings from an absorbing solution *IEICE Trans. Electron.* **E81-C** 455–61

[28] Deng L, He K, Zhou T and Li C 2005 Formation and evolution of far-field diffraction patterns of divergent and convergent Gaussian beams passing through self-focusing and self-defocusing media *J. Opt. A: Pure Appl. Opt.* **7** 409–15

[29] Iturbe Castillo M D, Sánchez-Mondragón J J and Stepanov S I 1995 Peculiarities of Z-scan technique in liquids with nonlinearity (steady regime) *Optik* **100** 49–56

[30] Reynoso Lara E, Navarrete Meza Z, Iturbe Castillo M D, Treviño Palacios C G, Marti Panameño E and Arroyo Carrasco M L 2007 Influence of the photoinduced focal length of a thin nonlinear material in the Z-scan technique *Opt. Express* **15** 2517–29

[31] Chapple P B, Staromlynska J, Hermann J A, Mckay T J and McDuff R G 1997 Single-beam z-scan: measurement techniques and analysis *Int. J. Nonlinear Opt. Phys.* **6** 251–93

[32] Porras Aguilar R, Ramirez-San Juan J C, Baldovino-Pantaleon O, May-Arrioja D, Arroyo Carrasco M L, Iturbe Castillo M D, Sanchez de la Llave D and Ramos Garcia R 2009 Polarization-controlled contrasted images using dye-doped nematic liquid crystals *Opt. Express* **17** 3417–23

[33] Sarkhos L, Aleali H, Karimzadeh R and Mansour N 2010 Large thermally induced nonlinear refraction of gold nanoparticles stabilized by cyclohexanone *Phys. Status Solidi* A **207** 2303–10